

# *Ab initio* molecular dynamics study of manganese porphine hydration and interaction with nitric oxide

Kevin Leung\* and Craig J. Medforth

Sandia National Laboratories,  
MS 1415 & 1349 Albuquerque, NM 87185

\*Email: kleung@sandia.gov

We use *ab initio* molecular dynamics (AIMD) and the DFT+U method to compute the hydration environment of the manganese ion in manganese (II) and manganese (III) porphines (MnP) dispersed in liquid water. These are intended as simple models for more complex water soluble porphyrins, which have important physiological and electrochemical applications. The manganese ion in Mn(II)P exhibits significant out-of-porphine plane displacement, and binds strongly to a single H<sub>2</sub>O molecule in liquid water. The Mn in Mn(III)P is on average coplanar with the porphine plane, and forms a stable complex with two H<sub>2</sub>O molecules. The residence times of these water molecules exceed 15 ps. The DFT+U method correctly predicts that water displaces NO from Mn(III)P-NO, but yields an ambiguous spin state for the MnP(II)-NO complex.

## I. INTRODUCTION

Porphyrins dispersed in water, coated on electrodes, and self-assembled into nanotubes have important applications as sensors<sup>1,2,3,4,5,6</sup> and light-induced water-splitting and hydrogen production.<sup>7</sup> Simple manganese porphyrins have been used as readily isolated experimental models for studying isoelectronic Fe(III) systems.<sup>8</sup> Water soluble Mn(II) and Mn(III) porphyrins are particularly useful for detection of nitric oxide in cell tissues, and for distinguishing them from nitroxyl (NO<sup>-</sup> and HNO) compounds.<sup>2,3</sup> The relaxation processes of water soluble manganese and iron *tetra-p*-sulfonatophenyl porphyrins (TSPP) in NMR-compatible time scales have also been the subject of significant experimental studies.<sup>9,10,11,12</sup>

Despite their importance and widespread appearance in technological and biological settings, theoretical studies of transition metal porphyrins in aqueous media have been rare. This is in part due to the difficulty of modeling transition metal systems in general. In liquid water, bare divalent and trivalent first row transition metal ions are octahedrally 6-coordinated due to their partially filled 3d electron shells. While density functional theory (DFT) successfully predicts this feature,<sup>13</sup> sophisticated classical force fields with 3-body terms or quantum mechanics/molecular mechanics methods are needed to reproduce such hydration structures.<sup>14,15</sup> Transition metal porphyrins present an inherently interesting case. The molecular framework has an overall -2e charge resulting from the nitrogen atoms chelating the metal ions. How these chelated ions in porphyrins interact with water will be affected by the ion size, spin state, and porphyrin conformations.

Predicting the spin state of transition metal porphyrins presents a considerable theoretical challenge. While DFT is formally exact, practical implementations depend on the choice of the approximate exchange correlation func-

tional, not all of which yield the correct spin state in transition metal complexes.<sup>16</sup> This is particularly true for first row transition metal porphyrins.<sup>17</sup> It has been shown that the hybrid functionals like B3LYP<sup>18</sup> yields the correct stable high spin ground state for manganese (II) porphine (Mn(II)P) and manganese (III) porphine (Mn(III)P),<sup>19</sup> while non-hybrid functionals like PBE,<sup>20</sup> lacking a long range Hartree-Fock exchange component, predict the incorrect intermediate spin state for Mn(II)P. If constrained to the high spin state, PBE still yields a poor Mn(II)P molecular geometry.<sup>19,21</sup> However, hybrid functionals are far more expensive to apply than non-hybrids when applying periodic boundary conditions appropriate to condensed phase systems such as liquid water or metal surfaces. This problem has been circumvented<sup>19</sup> by applying the DFT+U method on the Mn 3d electrons.<sup>24</sup> The screened coulomb ("U") term in DFT+U increases repulsion between electrons in low-spin, partially filled *d*-electron systems. In the approach used in Ref. 19, this term was parameterized using B3LYP spin splittings, and then the technique was applied to model MnP adsorbed on gold electrodes. The DFT+U method has also proved accurate for Fe-based catalysts.<sup>22</sup>

In this paper, we extend this previous work by conducting DFT+U based *ab initio* molecular dynamics (AIMD) simulations of Mn(II) and Mn(III) porphines in liquid water. Porphines not substituted with ionic side groups are mostly water-insoluble; our MnP molecules are intended as simple models for soluble porphyrins such as (MnTSPP),<sup>9,10,11</sup> which are too large and computationally costly to simulate using AIMD.<sup>23</sup> The elucidation of the hydration environment of the metal ion in porphyrins is a prerequisite for studying the binding of additional ligands to the metal site of water-soluble porphyrins. AIMD hydration studies are potentially useful for modeling electrochemical half-reactions involving porphyrins; such calculations have already been performed

for transition metal ions solvated in water.<sup>25</sup> Our work also suggests that the metal ion hydration structure assumed in the analysis of NMR relaxation experiments on Mn(II)TSPP may need to be re-examined.<sup>9,10</sup>

Finally, we briefly consider the binding between Mn(II)P and Mn(III)P and nitric oxide (NO) in the gas phase and in water. Such complexes are classified according to the format  $\{\text{MNO}\}^n$ ,<sup>26</sup> where  $n$  is the number of metal  $d$ -electrons plus the unpaired electron contributed by NO. For  $n \leq 6$ , the M-NO bond should be short ( $\sim 1.65$  Å), and the M-N-O angle should be  $\sim 180^\circ$ .<sup>26</sup> Mn(II) porphyrins are  $n = 6$  complexes, and X-ray structures of Mn(II) porphyrins ligated to NO indeed exhibit bond lengths and angles appropriate to  $\{\text{MNO}\}$ .<sup>6,8,27</sup> To our knowledge, no X-ray structures of NO-ligated Mn(III) porphyrins have been reported. Water soluble Mn(III) porphyrins are found not to complex with NO in aqueous conditions.<sup>4</sup> As a result, electrochemical switching of the Mn oxidation state is potentially useful for detecting NO in cell tissues, and in distinguishing NO from HNO, which binds to Mn porphyrins in both oxidation states.

Ideally, the same DFT method and/or functional can be used to predict all properties (energetics, structures, spectral properties) in all aqueous phase applications. There have been several reported successes of DFT treatment of Fe porphyrin-NO complexes.<sup>28,29</sup> These studies have focused on the molecular structures and vibrational properties, and not the binding energies between porphyrins and nitric oxide. In this work, we critically examine the effect of applying different exchange-correlation functionals on the spin state, molecular geometry, and binding energies of MnP-NO. We find that the DFT+U method successfully predicts that the Mn(III)P-NO complex dissociates in liquid water environments. However, we also conclude that neither DFT+U nor existing, widely used DFT functionals enjoy universal success in modeling nitric oxide ligation. This suggests that substantial functional development and refinement are necessary.

This paper is organized as follows. Section 2 describes the method used. Section 3 discusses the structure of water around the manganese ions in porphyrins. MnP-NO binding is briefly described in Sec. 4, and Sec. 5 concludes the paper with further discussion.

## II. METHODS

We conduct *ab initio* molecular dynamics (AIMD) based on the DFT+U<sup>24</sup> method implemented<sup>30</sup> in the VASP code version 4.6.<sup>31</sup> Our VASP calculations apply the PBE exchange correlation functional, the projected-augmented wave (PAW) method<sup>32</sup> and the standard VASP suite of PAW pseudopotentials. These include the Mn pseudopotential with pseudovalent  $2p$  electrons, and

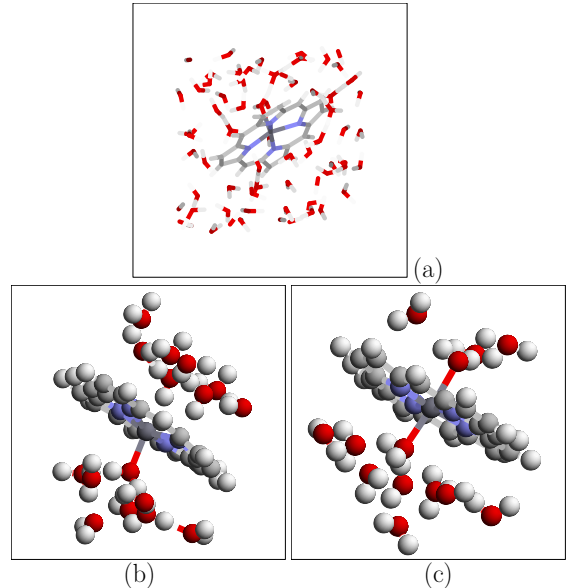


FIG. 1: Representative snapshots of (a) & (b) Mn(II)P in water; (c) Mn(III)P in water. Except in panel (a), only the water molecules close to the Mn ion are depicted.

the oxygen, carbon, nitrogen, and hydrogen pseudopotentials with default energy cutoffs of 400, 400, 400, and 250 eV, respectively.

The Mn 3d orbitals are augmented with screened column (“ $U$ ”) and exchange (“ $J$ ”) terms of  $U = 4.2$  and  $J = 1.0$  eV, respectively. These values have been shown to reproduce Mn(II)P high-spin/intermediate spin splittings predicted by the B3LYP functional,<sup>19</sup> and predict the high spin Mn(III) porphyrin spin state observed in experiments. For more details, see Ref. 19 and the supporting information therein.

A plane wave energy cut-off of 400 eV and a wavefunction convergent criterion of  $10^{-5}$  eV at each of the 0.5 ps time step in the Born-Oppenheimer AIMD simulations. This work focuses on structural properties; hence, deuterium is substituted for all protons so that a larger time step can be used. A Nose thermostat with an estimated time constant of 20 fs maintains the average temperature at  $T=375$  K. With these parameters, the drift in total energy is 0.9 Kelvin per picosecond (i.e.,  $\sim 0.004$  mHt/atom/ps) or less. This small energy drift is absorbed by the thermostat. Since the underlying PBE exchange correlation functional yields overstructured water and slow dynamics at  $T=300$  K,<sup>33</sup> the elevated temperature is necessary to obtain reasonable water structure and diffusion timescales. (See discussions in the next section.) These factors imply that the trajectories do not capture the real-time dynamics. Instead, the time dependence observed is used to confirm that the system has reached equilibrium, and it provides a time scale for

thermal fluctuations under these simulation conditions. Trajectory lengths of at least 15 ps are used to collect statistics after equilibration runs have stabilized the potential energy.

The simulation cell is cubic with a linear dimension of 13.65 Å. The planar porphine molecule is inserted diagonally into the cell. This ensures that there are 5 to 6 layers of water molecules separating the periodically replicated MnP in the direction perpendicular to the porphine ring (Fig. 1). The water density in the cell is determined using a grand canonical Monte Carlo (GCMC) simulation, using the Towhee code,<sup>34</sup> SPC/E rigid water molecule force fields,<sup>35</sup> and porphine force fields appropriate for NiP,<sup>36</sup> which, with the exception of the metal ion parameters, should be reasonable for porphine atom-H<sub>2</sub>O interactions. The Mn(II)P is held frozen in place in the GCMC simulations. It is found that 70 water molecules reside in the simulation cell. In the absence of Mn(II)P, the 13.65 Å<sup>3</sup> cubic cell would contain 85 water molecules at 1.0 g/cc density.

The water content for Mn(II)P-NO is similarly determined using GCMC, resulting in 68 H<sub>2</sub>O molecules in the simulation cell. The nitric oxide force field used is similar to that of Ref. 37. NO is essentially a hydrophobic molecule that interacts weakly with water.

All liquid phase pair correlation functions  $g(r)$  are computed with a 0.1 Å bin size, except that a 0.05 Å bin size is used for pure liquid water.

B3LYP hybrid functional<sup>18</sup> calculations of gas phase porphine complexes are performed using the program Gaussian 03.<sup>38</sup> We first optimize the geometries using the LANL2DZ basis set. Then we switch to the more accurate 6-311+G(d,p) basis, and perform geometric optimization for 3 to 5 steps until the magnitude of each Cartesian component of the force on each atom is below  $\sim 0.05$  eV/Å. (VASP gas phase calculations utilize a similar criterion for attaining optimal geometry.) We find that the PBE Mn(II)P-H<sub>2</sub>O binding energy computed using the 6-311+G(d,p) basis set, and that computed using the VASP code with plane wave basis sets, agree to within 24 meV.

### III. HYDRATION STRUCTURES OF MANGANESE PORPHINES

First we consider the hydration structure of Mn(II)P in water. Simple, electrostatic-plus-Lennard Jones interactions between water and the porphine molecule are applied during the GCMC pre-equilibration simulation. These force fields predict that a H<sub>2</sub>O ligates to the metal ion on each side of the porphine plane, but the overall metal coordination structure is strongly distorted from the ideal octahedral geometry. Applying AIMD on this classical force field-generated starting configuration leads to substantial structural changes. We find that a 8 ps

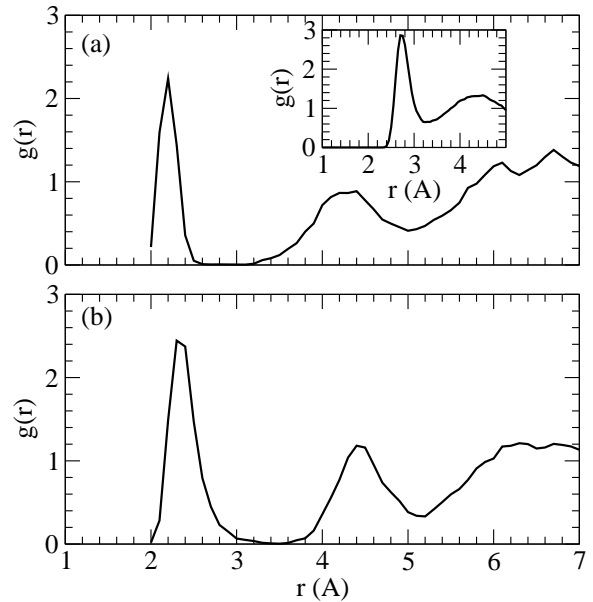


FIG. 2: Pair correlation functions  $g(r)$  between the Mn ion and the oxygen sites of H<sub>2</sub>O for (a) Mn(II)P; (b) Mn(III)P. Inset:  $g_{OO}(r)$  for liquid water.

AIMD trajectory is needed to equilibrate the potential energy of the system. AIMD simulation of Mn(III)P in water is started from an equilibrated Mn(II)P configuration, and the potential energy of the system also converges to a plateau value within 8 ps. These long equilibration times help ensure that the statistics collected in the subsequent 15 ps production run are independent of initial conditions.

Figure 1a depicts a equilibrated hydration structure around Mn(II)P and confirms that there are several layers of water molecules buffering the Mn ion from its periodic image. This suggests that the hydration environment of the Mn ion adequately represents bulk water boundary conditions.

The representative configuration depicted in Fig. 1b focuses on H<sub>2</sub>O close to the Mn ion. Unlike the classical force field results, the Mn ion in Mn(II)P strongly binds to one rather than two H<sub>2</sub>O molecules. As discussed below, this can be related to the significant out of porphine plane motion exhibited by the Mn(II) ion. Figure 1c depicts Mn(III)P in water. Mn(III)P is on average coplanar with the porphine plane, and the Mn binds to two water molecules. These snapshots encapsulate this section's main results, which will be analyzed in some detail below.

The Mn(II)-H<sub>2</sub>O pair correlation function  $g_{\text{Mn}-\text{O}_w}(r)$  is plotted in Fig. 2a, and it confirms the structure shown in Fig. 1b. The first peak in the Mn-O<sub>w</sub>  $g(r)$  integrates to 1.0 from  $r = 0$  to  $r = 3.0$  Å, which is the first  $g(r)$  minimum. The sharp peak and deep minimum clearly show that this water molecule is strongly bound to the

Mn(II) ion. They are reminiscent of divalent cation  $g(r)$  in liquid water.<sup>15,39</sup> In fact, over the entire 15 ps production run trajectory, the same water molecule remains bound to the Mn ion, although during the 8 ps equilibration trajectory, exchange of Mn first hydration shell water molecules with the bulk water region has occurred. Experimentally, the time scale for proton exchange that involves  $\text{H}_2\text{O}$  bound to Mn(II) is known to be on the order  $10^{-8}$  to  $10^{-7}$  s.<sup>40</sup>

The inset to Fig. 2 depicts the pure water  $g_{\text{OO}}(r)$ , computed using the PBE functional, 32 water molecules at 1.00 g/cc light water density, and with the thermostat set at  $T=375$  K. It confirms that PBE water at  $T=375$  K exhibits less overstructuring compared to PBE water at  $T=300$  K. For example, the  $g_{\text{OO}}(r)$  first peak exhibits a peak height of 2.9 density units at  $T=375$  K, which is in reasonable agreement with the value of 3.1 reported by Sit *et al.*<sup>41</sup> The small discrepancy can be attributed to statistical uncertainties and/or the use of different bin sizes. In contrast, at  $T=300$  K, this peak height exceeds 3.4 density units,<sup>42</sup> which is considerable larger than the experimental value.<sup>41</sup> Our choice of  $T=375$  K is thus reasonable for MnP hydration studies. While we have imposed a water density estimated using classical force fields and the GCMC method, we note that ion hydration structure appears insensitive to significant variations ( $\sim 7\%$ ) in water density.<sup>43</sup>

The stability of the single- $\text{H}_2\text{O}$  coordination structure of Mn(II)P is closely related to the significant Mn out-of-plane motion. Figure 3a depicts the evolution of this displacement along the AIMD trajectory. Here, at each time step, we perform a least square-fit to generate a plane,  $ax + by + cz = 1$ , through the 4 nitrogen atoms, and  $\delta_{\text{Mn}}$  is obtained as the smallest distance between the Mn atom and this plane. On average,  $\delta_{\text{Mn}}$  is 0.48 Å for Mn(II)P dispersed in water.

This large displacement can be related to the extremely flat out-of-plane Mn potential energy surface predicted by the DFT+U method for high spin Mn(II)P in the gas phase (Fig. 3b). Thus, upon binding to a ligand like a  $\text{H}_2\text{O}$ , the Mn ion is readily displaced out of the porphine plane. We find that this displacement is already 0.225 Å for the Mn(II)P- $\text{H}_2\text{O}$  complex in the gas phase, and this geometric feature explains the inability of the Mn ion to bind to a second  $\text{H}_2\text{O}$  in a liquid water environment. Note that the out-of-plane displacement of the Mn ion is accompanied by only a small amount out-of-plane deformation of the porphine ring (approximately 0.1 Å total deformation as determined by Normal Coordinate Structure Decomposition; see Table S1).

The out-of-plane Mn motion exhibits a flat potential energy surface because the high spin Mn(II) ion has a large effective size. The Mn-N distance in high spin Mn(II)P is predicted to be 2.09 Å, in good agreement with experiments.<sup>45,46</sup> Thus, energetically, it is relatively unfavorable for Mn to fit in the center of the ion-chelating

site of the porphine molecule. In contrast, the Mn(III) ion is smaller, with an Mn-N distance of 2.045 Å in MnCIP,<sup>19</sup> and in isolated Mn(III)P strongly prefers to be coplanar with the porphine plane (Fig. 3c). In liquid water, this preference persists on average (Fig. 3a). This geometry allows effective binding to two ligands. Indeed the sharply peaked Mn-water first peak in  $g(r)$  integrates to 2.0, indicating two  $\text{H}_2\text{O}$  are strongly ligated to the Mn ion. We do not observe exchange of the two  $\text{H}_2\text{O}$  molecules bound to the Mn(III) ion with outer shell water during the 15 ps trajectory.

A search of the Cambridge Crystallographic Data Center (CCDC) yields 15 crystal structures of Mn porphyrins with one or more coordinated water molecules. The manganese ion exhibits the +3 oxidation state in all of them. The experimentally determined Mn-O distances in the Mn(III) porphyrins ( $\sim 2.2$  Å) correspond closely to the first peaks in the pair correlation functions in Fig. 2. The average calculated Mn-N(porphine) distance in the high-spin ( $m = 2$ ) Mn(III)P( $\text{H}_2\text{O}$ )<sub>2</sub> energy minimized using the DFT+U is 2.028 Å. This again agrees well with the Mn-N(porphyrin) distances observed in Mn(III) porphyrin complexes with two axial water ligands (e.g., Mn(III)TPP( $\text{H}_2\text{O}$ )<sub>2</sub>(BPh)<sub>4</sub>, where the Mn-N distance is 2.011 Å).<sup>47</sup> The porphine ring again shows very little non-planar distortion in either the DFT+U gas phase structure of Mn(III)P( $\text{H}_2\text{O}$ )<sub>2</sub> (Table S2) or the crystal structure of Mn(III)TPP( $\text{H}_2\text{O}$ )<sub>2</sub>(Bph)<sub>4</sub> (Table S3).

Gas phase B3LYP and DFT+U calculations of the MnP-( $\text{H}_2\text{O}$ )<sub>2</sub> complex (Fig. 4, Table I) provide more compelling evidence that Mn in Mn(II)P coordinates to only one water molecule. Both these methods predict that there are two nearly isoenergetic configurations for the high spin Mn(II)P-( $\text{H}_2\text{O}$ )<sub>2</sub> cluster (Fig. 4). The bidentate Mn(II) configuration, with the Mn ion residing in the porphine plane (Fig. 4a), is only slightly more stable than the one where Mn(II) is  $\sim 0.4$  Å out-of-plane and one  $\text{H}_2\text{O}$  is bound to Mn and the other coordinated to two nitrogen atoms (Fig. 4b). DFT+U predicts that the bidentate configuration is more stable by only 15 meV, while B3LYP predicts that they are equally stable. In contrast, with the system in either the intermediate or the high spin state, PBE predicts that the structure depicted in Fig. 4b is *unstable* and spontaneously relaxes to that shown in Fig. 4a. This emphasizes that there are fundamental differences between DFT+U and PBE predictions for gas phase properties. These differences carry over into liquid phase AIMD simulations (Fig. 1a) favoring configurations similar to Fig. 4b.<sup>48</sup>

Because of the slow exchange rate of Mn first hydration shell  $\text{H}_2\text{O}$ , it is important to check whether the Mn(II)P hydration structure we observe depends on the initial configurations. Thus, we start with a equilibrated Mn(III)P configuration, with two water molecules ligated to the Mn ion, and initiate a Mn(II)P AIMD simulation by adding one more electron to the simulation

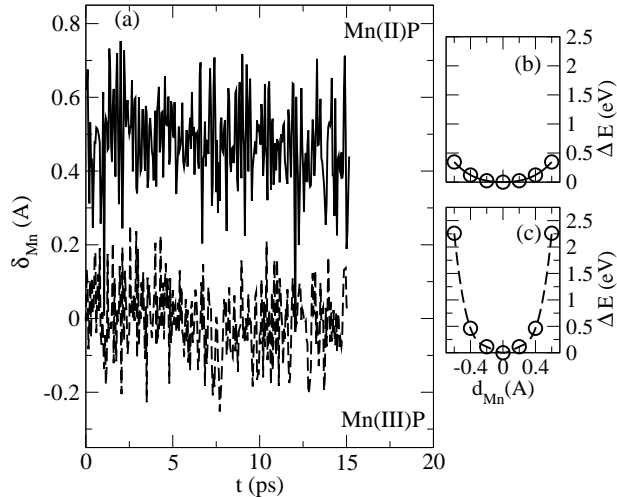


FIG. 3: (a) Out-of-porphine plane displacement of Mn ion,  $\delta_{\text{Mn}}$ , over the AIMD trajectories for Mn(II)P and Mn(III)P. (b) & (c) Energies as functions of Mn out-of-plane displacement in the gas phase for Mn(II)P and Mn(III)P, respectively. The porphine ring is held fixed as the Mn is displaced.

cell. Within 1 ps, one of the first hydration  $\text{H}_2\text{O}$  detaches itself, the Mn ion exhibits strong out-of-plane displacement, and the single  $\text{H}_2\text{O}$  hydrated, 5-coordinated Mn(II) configuration is recovered. Thus, this Mn(II)P hydration structure is robust.

The predicted hydration structure of Mn(II)P might possibly resolve anomalies associated with paramagnetic relaxation behavior of Mn(II)TPPS in water.<sup>10,11</sup> One model proposed in the NMR literature assumes a 6-coordinated geometry, where 2 axial  $\text{H}_2\text{O}$  molecules bind to the manganese ion in Mn(II)TPPS.<sup>11</sup> In contrast, AIMD predicts only one  $\text{H}_2\text{O}$  in the hydration shell and a breaking of the inversion symmetry about the porphine plane, which now exhibits a  $C_{4v}$  symmetry. This suggests that the underlying assumptions of Ref. 11 regarding coordination to water may need to be re-examined. While paramagnetic relaxation behavior is complex, we propose that using a model with the Mn ion ligated to the AIMD predicted number of water molecules might improve agreement between experiments and the spin-Hamiltonian results used to interpret NMR data.<sup>10,11</sup>

Figure 5 examines the hydration environment of the four nitrogen atoms surrounding the Mn ion. Integrating the  $g_{\text{N-O}_w}(r)$  to its first minimum (3.8 and 3.9 Å for Mn(II)P and Mn(III)P respectively), we find that there are 1.76 and 2.83  $\text{H}_2\text{O}$  in the hydration shell of each nitrogen atom. These spatial correlations partly originate from the one (two)  $\text{H}_2\text{O}$  strongly coordinated to the Mn(II) (Mn(III)) ion in the vicinity of the nitrogen atoms, and not from water-nitrogen hydrogen bonding. A N-H hydrogen bond typically exhibits a  $g_{\text{N-H}_w}(r)$  peak at  $r \sim 1.8$  Å, and a first minimum at  $r \sim 2.5$  Å.<sup>49</sup>

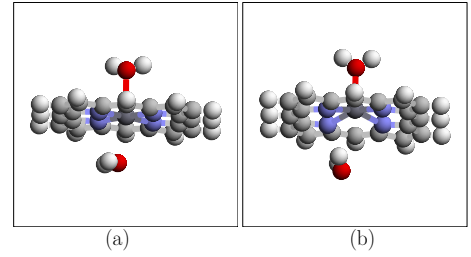


FIG. 4: Two configurations of Mn(II)P- $(\text{H}_2\text{O})_2$ . DFT+U and B3LYP both predict that they are similar in energy, while PBE predicts that the structure in (b) is unstable.

Here,  $g_{\text{N-H}_w}(r)$  only exhibits small shoulders. Integrating  $g_{\text{N-H}_w}(r)$  to  $r = 2.5$  Å yields only 0.10 and 0.02  $\text{H}_2\text{O}$  in the first coordination shell per nitrogen atom for Mn(II)P and Mn(III)P, respectively. We conclude that water interacts weakly with the nitrogen atoms.

Note that our AIMD trajectories impose a high spin configuration, known to be favorable in the gas phase.<sup>19</sup> We have tested snapshots of the Mn(II)P trajectory to see if Mn(II)P in water favors spin states at variance from those predicted for the gas phase ground state. We invariably observe that the high spin configuration is favorable in these DFT+U generated AIMD snapshots when using the DFT+U technique, in agreement with experiments on MnTSP in water.<sup>10,11</sup> The intermediate spin state is favored in these snapshots when the PBE functional is used. Thus, dispersing Mn(II)P into liquid water does not alter the most stable spin state; for each functional used, the gas phase and aqueous phase spin state predictions are in agreement. This is expected because water is not a strong ligand.

#### IV. INTERACTIONS WITH NITRIC OXIDE

In this section, we examine the interaction of Mn(II)P and Mn(III)P with NO. Ideally, the DFT+U method, which predicts the correct  $s = 5/2$  spin state for Mn(II)P, can be used to treat MnP-NO binding in aqueous environments. We will show that DFT+U appears to yield reasonable binding energies. Neither DFT+U nor B3LYP necessarily predicts the correct spin states for the MnP-NO complexes. However, since the energies of different spin states are so similar, our conclusions concerning binding energies appear to be robust.

We first consider gas phase predictions. Table I depicts the PBE, B3LYP, and DFT+U results based on the PBE functional and  $U = 4.2$  eV,  $J = 1.0$  eV. Here we use the notation  $m$  to denote the magnetic moment of the entire complex in the simulation cell.

Species	Ligand	$m$	PBE	B3LYP	DFT+U
Mn(II)P	NO	0	-2.031	-0.524	-0.607
Mn(II)P	NO	1	-1.687	-0.728	-0.930
Mn(II)P	NO	2	NA	-0.022	-0.407
Mn(III)P	NO	1/2	-1.302	0.000*	+0.030*
Mn(III)P	NO	3/2	-0.651	-0.322	-0.401
Mn(III)P	NO	5/2	-0.103	-0.077	-0.163
Mn(II)P	H <sub>2</sub> O	5/2	NA	-0.359	-0.345
Mn(II)P	H <sub>2</sub> O	3/2	-0.283	NA	NA
Mn(II)P	2 H <sub>2</sub> O	5/2	NA	-0.487	-0.516
Mn(II)P	2 H <sub>2</sub> O	3/2	-0.457	NA	NA
Mn(II)P	NO + H <sub>2</sub> O	1	NA	NA	-0.886
Mn(II)P	NO + H <sub>2</sub> O	0	-2.309	NA	NA
Mn(III)P	H <sub>2</sub> O	2	-0.571	-0.629	-0.581
Mn(III)P	2 H <sub>2</sub> O	2	-0.997	-1.045	-0.946
Mn(III)P	NO + H <sub>2</sub> O	3/2	NA	NA	-0.590
Mn(III)P	NO + H <sub>2</sub> O	1/2	-1.854	NA	NA

TABLE I: Binding energies between MnP and NO or H<sub>2</sub>O, in eV.<sup>44</sup> PBE and DFT+U results utilizes planar wave basis while B3LYP calculations are performed using the 6-311+(d,p) basis.  $m$  is the total magnetic polarization in the complex. In some cases only the results for the most stable spin state predicted for each DFT functional are listed. \*Negligible binding energy predicted.

### A. Mn(II)P-NO

PBE correctly predicts a low spin ground state for Mn(II)P-NO, with a 1.617 Å Mn-N (nitric oxide) bond length, and a Mn-N-O angle of 173.6°. The Mn ion is displaced 0.342 Å out of the porphine plane, and the porphine ring shows little evidence of non-planar deformation ( $\sim 0.1$  Å, see Table S4). These predictions are in good agreement with the X-ray structure for nitrosyl(5,10,15,20-tetratolylporphinato) manganese (Mn(TTP)NO), which reveals a 1.641 Å Mn-NO bond length, a 177.8° M-N-O angle, and a 0.337 Å Mn out-of-plane displacement.<sup>8,26,27</sup> The four other Mn(II)tetraarylporphyrins in the CCDC are 6-coordinated but show similar Mn-NO distances (1.645-1.680 Å). The average Mn-N(porphyrin) distance in the PBE structure of Mn(II)P-NO is 2.022 Å, which compares favorably with the crystal structure distance of 2.004 Å.<sup>26</sup> The crystal structure of Mn(II)TPP-NO also shows a modest amount of non-planar deformation ( $\sim 1.2$  Å, Table S5) which may in part explain the slightly shorter Mn-N (porphyrin) distance. PBE predicts a large (2.03 eV) MnP-NO binding energy (Table I).

DFT+U and B3LYP results are qualitatively and even quantitatively similar to each other but disagree with the experimental data. They predict, incorrectly, that the  $m = 1$ , intermediate spin configuration is more stable than the low spin state, by 0.20 and 0.32 eV, respec-

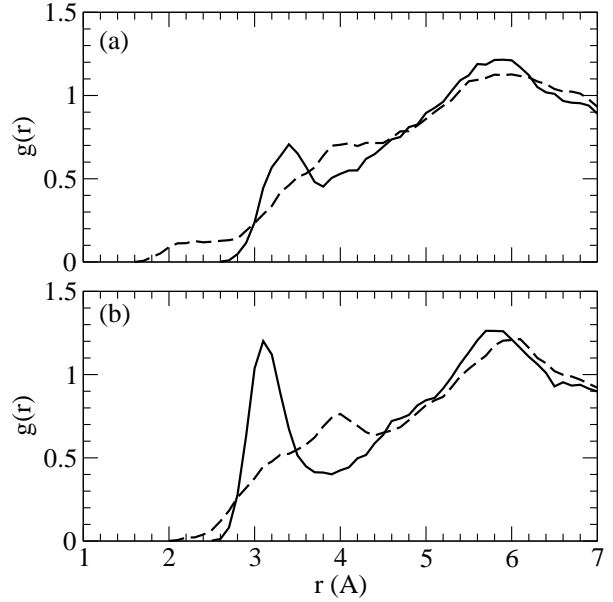


FIG. 5: Pair correlation functions,  $g_{N-O_w}(r)$  (solid lines) and  $g_{N-H_w}(r)$  (dashed lines), between the nitrogen atoms and the oxygen/hydrogen sites of H<sub>2</sub>O for (a) Mn(II)P; (b) Mn(III)P.

tively. For this ground state, the Mn-N<sub>NO</sub> distance is 1.91 (1.89) Å the Mn-N-O angle is 142.2 (144.2)°, the out-of-plane Mn displacement is 0.277 (0.323) Å, and the MnP-NO binding energy is 0.93 (0.73) eV. DFT+U further predicts that the low-spin configuration still exhibits a considerable binding energy of 0.61 eV, with a 1.766 Å Mn-NO bond length and 174° M-N-O bond angle, respectively.

We note that Gaussian B3LYP calculations reveal some spin-contamination for the  $m = 1$  intermediate spin state. The VASP package does not calculate spin contaminations, but it is likely that VASP-based DFT+U calculations also contain a similar degree of spin-contamination for this spin state. We emphasize that only the NO-ligated species exhibit such a contamination. Since both the energies of the  $m = 0$  and  $m = 1$  spin states agree to within 0.3 eV, the order of magnitude of our binding energies will likely not be strongly affected by the ambiguity regarding the spin state.

### B. Mn(III)P-NO

To our knowledge, no X-ray structures for NO-ligated Mn(III) porphyrins exist. Such hypothetical systems would be {M-NO}<sup>5</sup> complexes, which in principle should exhibit a low-spin ( $m = 1/2$ ), short Mn-N<sub>NO</sub>, linear Mn-N-O geometry.<sup>26</sup> PBE predicts such a low spin structure, but also yields an anomalously large MnP-NO binding energy of 1.30 eV (Table I; see below). This structure has an out-of-plane Mn displacement of 0.36 Å, which is

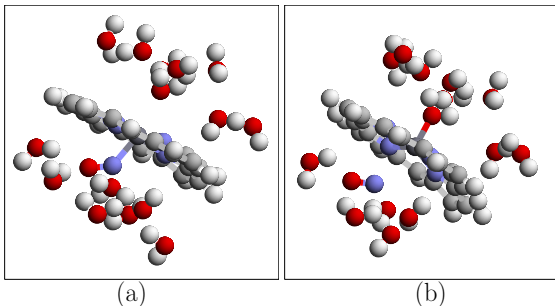


FIG. 6: Representative snapshots of (a) initial and (b) final configurations of the Mn(III)P-NO complex in water after 0.1 ps. Only H<sub>2</sub>O molecules close to the Mn ion are depicted.

comparable to that seen for low spin Mn(II)P-NO.

Both DFT+U and B3LYP predict negligible binding energies for NO with low spin Mn(III)P. The  $m = 3/2$  intermediate spin configuration, on the other hand, yields a small binding energy of 0.40 (0.32) eV and a small out-of-plane Mn displacement of 0.16 (0.10) Å. While no experimental data for binding energy is available, DFT+U predicts that the Mn(III)P-H<sub>2</sub>O complex is more favorable than the Mn(III)P-NO complex, while the reverse is true for PBE. This suggests that H<sub>2</sub>O will displace NO in a DFT+U based AIMD simulation, consistent with experiments on water-soluble Mn(III) porphyrins.<sup>2,3,4</sup> In contrast, because of the strong binding energy with NO, AIMD simulations based on the PBE exchange correlation functional will likely not lead to Mn(III)P-NO dissociation in water.<sup>50</sup>

Gaussian calculations again reveal some spin-contamination for both the  $m = 1/2$  and  $m = 3/2$  states. In contrast, no spin-contamination is observed for either Mn(II)P or Mn(III)P-Cl.<sup>19</sup> This underscores that MnP-NO systems are difficult to model using DFT methods.

### C. MnP-NO in water

Next, we investigate the stability of MnP-NO complexes in liquid water by conducting AIMD simulations. We pre-equilibrate hydrated Mn(II)P-NO configurations from a GCMC run as before, holding MnP-NO rigid in the DFT+U optimized, intermediate spin configuration, and then conduct AIMD simulations for 3 ps. Unlike for Mn(II)P ligated to H<sub>2</sub>O, the potential energy reaches a plateau on a sub-picosecond timescale. We find that the Mn ion in Mn(II)P-NO complex is stable in water, and does not ligate to any additional H<sub>2</sub>O molecules.

Next, we consider Mn(III)P-NO in water. Starting from an equilibrated aqueous Mn(II)P-NO configuration (Fig. 1d), we remove an electron from the simulation cell, and restart the DFT+U based AIMD trajectory with the

species	expt.	PBE	B3LYP	DFT+U
Mn(II)P	$s=5/2$	no	yes	yes
Mn(III)P	$s=2$	yes	yes	yes
Mn(II)P-NO	$s=0$	yes	no	no
Mn(III)P-NO	instability in water	no	NA	yes

TABLE II: Brief summary of the successes and failures of different DFT methods. Gas phase DFT and aqueous phase AIMD simulations that apply the same functional predict the same stable spin states in all cases considered.

spin polarization fixed at  $m = 3/2$ . Within 0.1 ps, the NO diffuses away from the Mn(III) ion, replaced by an H<sub>2</sub>O from the other side of the porphine plane (Fig. 1e; Fig. 6). Thus, DFT+U predicts that Mn(III)P fails to bind to NO in water, in agreement with experiments.<sup>2</sup>

To examine PBE predictions for Mn(III)P-NO, we use a DFT+U predicted Mn(III)P configuration in water, manually reposition the NO molecule to yield a 180° Mn-N-O angle and a 1.8 Å Mn-N bond length, impose a low spin ( $m = 1/2$ ) spin state, and restart the AIMD simulation using the PBE functional. We find that Mn(III)P-NO complex is stable in water over the course of a 5 ps trajectory. While these AIMD runs are short, their qualitative results are completely consistent with the relative stability of Mn(III)P-NO and Mn(III)P-H<sub>2</sub>O based on gas phase binding energy considerations (Table I). They show that PBE predictions are in apparent disagreement with experiments.<sup>2,3,51</sup>

### D. Summary of MnP-NO interactions

The apparent successes and failures of PBE and DFT+U methods in the gas and liquid phases are summarized in Table II. Recall that, in the absence of the NO ligand, PBE predicts an incorrect, intermediate Mn(II)P ( $s=3/2$ ) spin state while both B3LYP and DFT+U parameterized with B3LYP spin splittings predict the correct high spin ( $s=5/2$ ) state.<sup>19</sup> All three methods predict the correct spin state for Mn(III)P (high spin,  $s = 2$ ). The DFT+U method correctly predicts that the Mn(III)P-NO is unstable in liquid water. However, the spin state of the predicted stable species in the gas phase is inconsistent with the typical low-spin {M-NO}<sup>5</sup> structural parameters. PBE predicts that Mn(III)P-NO is a strongly bound complex, in apparent disagreement with aqueous phase experiments. For the Mn(II)P-NO structure, PBE predicts the experimental structure and spin state, while B3LYP and DFT+U do not.

Both the hybrid functional B3LYP and the DFT+U method favor the high-spin states of first row transition metal ion, by increasing the exchange interaction or screened coulomb interaction among 3d electrons. To a first approximation, when Mn and NO are far apart,

enforcing  $m = 0$  on the Mn(II)P-NO complex requires equal and opposite local  $s = 1/2$  spin moments on Mn and on the N atom of the NO molecule. We conjecture that DFT+U cannot reproduce the stability of  $m = 0$  Mn(II)P-NO because Mn(II)P strongly favors the high spin ( $m = 5/2$ ) state, while the low spin ( $m = 1/2$ ) state is highly unfavorable. In contrast, in PBE calculations the  $m = 1/2$  state is not extremely unfavorable in energy compared to  $m = 3/2$ , the stable Mn(II)P spin state erroneously predicted by PBE. Therefore, at least when Mn(II)P and NO are far apart, PBE predictions more readily accommodates a  $m = 0$  spin state.

In summary, state-of-the-art DFT methods are as yet unable to capture the delicate balance of competing effects and correlations that determine the stable spin state of Mn(II)P, Mn(III)P, and their nitric oxide complexes. NO ligation seems to be especially challenging due to  $\pi$ -electron back bonding.<sup>28,29</sup> The DFT+U method, with its most important parameter  $U$  fitted to the Mn(II)P high spin-intermediate spin splitting, should be further improved to take into account such  $\pi$ -back bonding.<sup>53</sup> These improvements may allow the more accurate prediction of binding energies, which have not been addressed in recent DFT work on porphyrin-nitric oxide complexes.<sup>28,29</sup>

## V. CONCLUSIONS

In this work, we have conducted *ab initio* molecular dynamics simulations of the hydration environment of the Mn ion in Mn(II)P and Mn(III)P dispersed in liquid water. These are intended as simple models of water-soluble manganese porphyrins. The DFT+U technique, parameterized with B3LYP spin splittings, successfully predicts that high spin Mn(II)P and Mn(III)P are stable in liquid water. Thus, this technique enables efficient molecular dynamics simulation of MnP with the correct spin state in a condensed phase environment. In contrast, the B3LYP functional, with its long range exchange, is costly to apply when using periodic boundary conditions.

The Mn ion in Mn(II)P is predicted to be displaced off-center out of the porphine plane by an average of 0.48 Å, and is ligated to a single H<sub>2</sub>O molecule. The Mn ion in Mn(III)P is on average co-planar within the porphine plane and binds strongly to 2 H<sub>2</sub>O molecules. Water molecules ligated to the Mn ion exhibit residence times of more than 15 ps. Water only interacts weakly with the nitrogen atoms on the porphine ring chelating the Mn ion. These predicted hydration structures might be potentially useful for improved analysis of NMR relax-

ation data.<sup>10,11</sup>

The application of DFT techniques to examine MnP-NO binding in both gas and aqueous phases proves less successful than for MnP dispersed in water. Ideally, the DFT+U technique, fit to B3LYP spin splittings for Mn(II)P and found to be successful for unligated MnP, should be applicable to all ligated complexes as well. Indeed, we find that DFT+U apparently succeeds in describing the binding energy of the Mn(III)P-NO complex. It predicts that the Mn(III)P-NO binding energy is substantially smaller than that for Mn(III)P-H<sub>2</sub>O. AIMD based on the DFT+U technique predicts a rapid dissociation of the Mn(III)P-NO in water, consistent with the known instability of Mn(III)P-NO in aqueous phase experiments.<sup>2,3</sup> Both DFT+U and B3LYP predict significantly larger Mn(II)P-NO binding energies than for Mn(III)P-NO. This differential ability of Mn(II) and Mn(III) porphyrins to ligate to NO is crucial for detecting NO in water and distinguishing NO from HNO or NO<sup>-</sup> via electrochemical means. In contrast, PBE predicts large ( $> 0.8$  eV) Mn-NO binding energies for both Mn(II)P-NO and Mn(III)P-NO, which would suggest, erroneously, that switching the oxidation state of MnP cannot trap and then release NO.

We emphasize that B3LYP and DFT+U predictions qualitatively agree with each other regarding Mn(II)P-NO binding, despite the fact that the DFT+U technique used herein is parameterized using B3LYP spin splitting for the bare Mn(II)P molecule. However, both these techniques predict incorrect spin states for the Mn(II)P-NO complex. On the other hand, the PBE functional predicts a Mn(II)P-NO low spin spin state and molecular geometry that are in good agreement with experiments.

While it is clear that more fundamental improvements to DFT methods need to be made, AIMD simulations based on the DFT+U technique successfully predicts many experimentally observed ligation features of Mn porphyrins, including the observation that complexes formed between Mn(III) porphyrins and nitric oxide are unstable in liquid water.

## Acknowledgements

We thank John Shelnett, Sameer Varma, and Prof. Robert Sharp for useful discussions. Sandia is a multiprogram laboratory operated by Sandia Corporation, a Lockheed Martin Company, for the U.S. Department of Energy's National Nuclear Security Administration under contract DE-AC04-94AL8500.

<sup>1</sup> Kadish, K. M.; Smith, K. M.; Guillard, R. *The Porphyrin Handbook* (Academic Press, San Diego, 2000).

<sup>2</sup> M. A. Marti, S. E. Bari, D. A. Estrin, and F. Doctorovich,

- J. Am. Chem. Soc. **127**, 4680 (2005).
- <sup>3</sup> J. Oni, N. Diab, I. Radtke, and W. Schuhmann, *Electrochimica Acta* **48**, 3349 (2003).
- <sup>4</sup> I. Spasojevic, I. Batinic-Haberle, and I. Fridovich, *Nitric Oxide: Biol. and Chem.* **4**, 526 (2000).
- <sup>5</sup> B. J. Vesper, K. Salaita, H. Zong, C. A. Mirkin, A. G. M. Barratt, and B. M. Hoffman, *J. Am. Chem. Soc.* **126**, 16653 (2004).
- <sup>6</sup> S. Yoshimoto, J. Inukai, A. Tada, T. Abe, T. Morimoto, A. Osuka, H. Furuta, and K. Itaya, *J. Phys. Chem. B* **108**, 1948 (2004).
- <sup>7</sup> Z. Wang, C. J. Medforth, and J. A. Shelnutt, *J. Am. Chem. Soc.* **126**, 16720 (2004).
- <sup>8</sup> W. R. Scheidt, K. Hatano, G. A. Rupprecht, and P. L. Piccolo, *Inorg. Chem.* **18**, 292 (1979).
- <sup>9</sup> N. Schaeffe and R. R. Sharp, *J. Chem. Phys.* **122**, 184501 (2005).
- <sup>10</sup> J. C. Miller and R. Sharp, *J. Phys. Chem. A* **104**, 4889 (2000).
- <sup>11</sup> L. H. Bryant, M. W. Hodges, and R. G. Bryant, *Inorg. Chem.* **38**, 1002 (1999).
- <sup>12</sup> N. Schaeffe and R. R. Sharp, *J. Phys. Chem. A* **109**, 3267 (2005).
- <sup>13</sup> D. Asthagiri, L. R. Pratt, M. E. Paulaitis, and S. B. Rempe, *J. Am. Chem. Soc.* **126**, 1285 (2004).
- <sup>14</sup> D. R. Nutt, M. Karplus, and M. Meuwly, *J. Phys. Chem. B* **109**, 21118 (2005).
- <sup>15</sup> B. M. Rode, C. F. Schwenk, T. S. Hofer, and B. R. Randolph, *Coord. Chem. Rev.* **249**, 2993 (2005).
- <sup>16</sup> M. Reiher, O. Salomon, and B. A. Hess, *Theor. Chem. Acc.* **107**, 48 (2001); M. Reiher, *Inorg. Chem.* **41**, 6928 (2002).
- <sup>17</sup> A. Ghosh and P. R. Taylor, *Curr. Opin. Chem. Biol.* **7**, 113 (2003).
- <sup>18</sup> A. D. Becke, *J. Chem. Phys.* **98**, 5648 (1993); C. T. Lee, W. T. Yang, and R. G. Parr, *Phys. Rev. B* **37**, 785 (1988).
- <sup>19</sup> K. Leung, S. B. Rempe, P. A. Schultz, E. M. Sproviero, V. S. Batista, M. E. Chandross, and C. J. Medforth, *J. Am. Chem. Soc.* **128**, 3659 (2006).
- <sup>20</sup> J. P. Perdew, K. Burke, and M. Ernzerhof, *Phys. Rev. Lett.* **77**, 3865 (1996).
- <sup>21</sup> Note that hybrid functionals such as B3LYP are not universally more successful than non-hybrid ones like PBE. A counter example is the case of transition metal dimers. See N. E. Schultz, Y. Zhao, D. G. Truhlar, *J. Phys. Chem. A* **109**, 4388 (2005) and references therein.
- <sup>22</sup> H. J. Kulik, M. Cococcioni, D. A. Scherlis, and N. Marzari, <http://arXiv.org/cond-matt/0608285> (2006)
- <sup>23</sup> The four negatively charged sulfonate groups in MnTSP ensure that the Mn ion is not ligated to anions in aqueous solutions, even if it is in the +3 oxidation state; hence we do not consider counter ions when modeling Mn(III)P in liquid water.
- <sup>24</sup> V. I. Anisimov, J. Zaanen, and O. K. Andersen, *Phys. Rev. B* **44**, 943 (1991); A. I. Liechtenstein, A. I. Anisimov, and J. Zaanen, *Phys. Rev. B* **52**, 5467 (1995).
- <sup>25</sup> Y. Tateyama, J. Blumberger, M. Sprik, and I. Tavernelli, *J. Chem. Phys.* **122**, 234505 (2005).
- <sup>26</sup> G. R. A. Wyllie and W. R. Scheidt, *Chem. Rev.* **102**, 1067 (2002), and references therein.
- <sup>27</sup> Z. N. Zahran, J. Lee, S. S. Alguindigue, M. A. Khan, and G. B. Richter-Addo, *Dalton Trans.* 44 (2004).
- <sup>28</sup> K. M. Vogel, P. M. Kozlowski, M. Z. Zgierski, and T. G. Spiro, *J. Am. Chem. Soc.* **121**, 9915 (1999).
- <sup>29</sup> T. Wondimagedn and A. Ghosh, *J. Am. Chem. Soc.* **123**, 5680 (2001).
- <sup>30</sup> O. Bengone, M. Alouani, P. Blöchl, and J. Hugel, *Phys. Rev. B* **62**, 16392 (2000).
- <sup>31</sup> G. Kresse and J. Furthmüller, *Phys. Rev. B* **54**, 11169 (1996); *Comput. Mater. Sci.* **6**, 15 (1996).
- <sup>32</sup> P. E. Blochl, *Phys. Rev. B* **50**, 17953 (1994); for VASP implementation, see G. Kresse and D. Joubert *Phys. Rev. B* **59**, 1758 (1999).
- <sup>33</sup> D. Asthagiri, L. R. Pratt, J. D. Kress, *Phys. Rev. E* **68**, 415051 (2003); J. C. Grossman, E. Schwegler, E. W. Draeger, F. Gygi, G. Galli, *J. Chem. Phys.* **120**, 300 (2004); J. VandeVondele, F. Mohamed, M. Krack, J. Hutter, M. Sprik, M. Parrinello, *J. Chem. Phys.* **122**, 014515 (2005).
- <sup>34</sup> M. G. Martin and A. P. Thompson, *Fluid Phase Equil.* **217**, 105 (2004).
- <sup>35</sup> H. J. C. Berendsen, J. R. Gridera, and T. P. Straatsma, *J. Phys. Chem.* **91**, 6269 (1987).
- <sup>36</sup> X.-Z. Song, L. Jaquinod, W. Jentzen, D. J. Nurco, S.-L. Jia, R. G. Khoury, J.-G. Ma, C. J. Medforth, K. M. Smith, and J. A. Shelnutt, *Inorg. Chem.* **37**, 2009 (1998); J. A. Shelnutt, C. J. Medforth, M. D. Berber, K. M. Barkigia, and K. M. Smith, *J. Am. Chem. Soc.* **113**, 4077 (1991).
- <sup>37</sup> Z.-W. Zhou, B. D. Todd, K. P. Travis, and R. J. Sadus, *J. Chem. Phys.* **123**, 054505 (2005).
- <sup>38</sup> M. J. Frisch, *et al.*, Gaussian 03 (Revision C.02), Gaussian Inc., (Wallingford, CT, 2004).
- <sup>39</sup> D. Asthagiri and L. R. Pratt, *Chem. Phys. Lett.* **371**, 613 (2003).
- <sup>40</sup> Z. Luz and R. G. Shulman, *J. Chem. Phys.* **43**, 3750 (1965); R. A. Bernheim, T. H. Brown, H. S. Gutowsky, and D. E. Woessner, *J. Chem. Phys.* **30**, 950 (1959).
- <sup>41</sup> P. H.-L. Sit and Ni. Marzari, *J. Chem. Phys.* **122**, 204510 (2005).
- <sup>42</sup> E. Schwegler, J. C. Grossman, F. Gygi, and G. Galli, *J. Chem. Phys.* **121**, 5400 (2004).
- <sup>43</sup> K. Leung and S. B. Rempe, *Phys. Chem. Chem. Phys.* **8**, 2153 (2006).
- <sup>44</sup> These energies do not include zero point energy (ZPE) corrections. We have not computed ZPE for MnP, but we note that the FeP-NO vibration frequency has been shown to be small, on the order of 550 cm<sup>-1</sup>,<sup>28</sup> which implies a ZPE of at most 2 kcal/mol.
- <sup>45</sup> J. F. Kirner, C. A. Reed, W. R. Scheidt, *J. Am. Chem. Soc.* **99**, 1093 (1977).
- <sup>46</sup> B. Cheng, W. R. Scheidt, *Acta Crystallogr. C* **52**, 361 (1996).
- <sup>47</sup> P. Turner, M. J. Gunter, B. W. Skelton, A. H. White, and T. W. Hambley, *J. Chem. Res.* **18**, 220 (1996).
- <sup>48</sup> Indeed, our preliminary PBE based AIMD simulations, with the simulation cell constrained to  $m = 5/2$ , show that PBE predicts a much higher tendency towards Mn(II) binding to two water molecules, and the Mn(II) ion residing in the porphine plane.
- <sup>49</sup> See, e.g., K. Leung, *Biophys. Chem.* (in press).
- <sup>50</sup> To make this point more precise, note that the previous

section shows that Mn(III)P binds to two H<sub>2</sub>O in liquid water. Therefore we should compare the PBE energies of Mn(III)P(NO)(H<sub>2</sub>O) and Mn(III)P(H<sub>2</sub>O)<sub>2</sub>. Table I indicates that that, in the gas phase, the former is more favorable by 0.857 eV, or 19.75 kcal/mol.<sup>44</sup> This is an underestimate of the energetic preference for Mn(III)P(NO)(H<sub>2</sub>O) in liquid water, because replacing a NO ligand with H<sub>2</sub>O from the bulk water region involves breaking two hydrogen bonds and moving a hydrophobic species (NO) into bulk water. At T=300 K, one can readily estimate that the translational entropy advantage of dissociating Mn(III)P-NO in a 1  $\mu$ M NO solution is  $\sim$  11 kcal/mol. This entropic gain is too small to offset the binding energy cost for dissociation. Thus, by any reasonable measure, PBE erroneously predicts that the Mn(III)P(NO) complex does not dissociates in liquid water.

<sup>51</sup> The dynamics of dissociation can be extremely complex and may involve spin-forbidden transitions.<sup>52</sup> Studying

Mn(II)P-NO dissociation is not the main objective of this work.

<sup>52</sup> J. N. Harvey, J. Am. Chem. Soc. **122**, 12401 (2000).

<sup>53</sup> We have not found values of  $U$  within the DFT+U approach that yield both a high spin ground state for Mn(II)P and a low spin ground state for Mn(II)P-NO. This suggests that dynamic electronic correlation effects, not accounted for by the static DFT+U method, may be important in Mn(II)P-NO.

<sup>54</sup> See EPAPS Document No. XXXX for supplemental information on normal-coordinate structure decomposition (NSD) analysis of several computed and experimental porphyrin structures. This document may be retrieved via the EPAPS homepage (<http://www.aip.org/pubservs/epaps.html>) or from <ftp.aip.org> in the directory /epaps/. See the EPAPS homepage for more information.